**communications** earth & environment

A Nature Portfolio journal

Article

https://doi.org/10.1038/s43247-026-03645-2

# Neglected shoreward reintroduction of pre-aged sedimentary organic carbon in a large river- and tide-dominated marginal sea

Check for updates

**Lilei Chen[1], Feng Li[2], Jian Liu[2] ✉, Yoshiki Saito[3], Shuwen Sun[1], Jiandong Qiu[2], Xingliang He[2], Bin Chen[2], Gang Tong[4] & Maogang Qin[5]**

The coastal to inner-shelf muddy belt and offshore tidal sand ridges of the East China Sea (ECS) constitute a coupled sedimentary pattern during the postglacial deposition, challenging the prevailing paradigm of seaward, unidirectional dispersal of sedimentary organic carbon (OC) in coastal to shelf regions worldwide. Here we investigate characteristics and temporal heterogeneity of diverse sedimentary OC in specific depositional environments during the past 14 kyr based on dual carbon isotopes ($^{13}C$ and $^{14}C$) and multi-biomarkers in sediment core ECS-1302 of the muddy belt. Sedimentary OC-$^{14}C$ ages deviated anomalously from their depositional ages during the postglacial transgression, alongside a decreasing proportion of terrestrial OC, supporting energetic forcing reintroduced pre-aged OC from offshore into coastal to inner-shelf areas, associating with shoreward, fine-grained sediment reworking of the paleo-Yangtze River estuary. This study underscores dual-directional cycles of sedimentary OC should be fully considered in exploring carbon cycle for large river- and tide-dominated marginal seas.

Sedimentary organic carbon (OC) recycling of continental shelves plays a crucial role in the movement of carbon from short-term surface processes to the long-term geological cycle[1,2]. This is because continental shelves preserve approximately 80% of OC burial in sediments, even though they occupy only 7–10% of global ocean area[1]. To date, numerous studies have been devoted to depicting the source, transport, and fate of terrestrial OC along the land-ocean continuum paths via seaward cross-shelf dispersal and alongshore advection over modern timescales[3–6]. These studies have underlined the importance of small rivers and/or atmospheric deposition for pre-aged OC loadings[7], as well as the exposure of aged OC by gravity-driven flows and the potential transport of this re-exposed OC to the interior ocean[8]. Other studies have tied sea-level and climatic changes to the fate of contemporary terrigenous OC in the recent geological past[9–11]. However, the contribution of reintroduced, dormant OC that first accumulated on the middle and outer shelf throughout glacial to interglacial cycles, especially during marine transgressions, has been overlooked in shallow and vast marginal seas[12–14].

The East China Sea (ECS) is characterized by a dominant interaction between the Yangtze River and strong tidal currents. The coastal to inner-shelf muddy belt of the ECS occurs in waters typically shallower than about 60 m and is composed mainly of clayey silt and silty clay (Fig. 1). These sediments are dominated by terrestrial material from the Yangtze River, and are associated with a high sedimentation rate and high marine primary productivity[15,16]. Adjacent to the inner shelf, coarse-grained, active, moribund, and buried tidal sand ridges (Fig. 1) have developed widely since the last deglaciation on the middle and outer shelf of the ECS under strong tidal currents. This process is accompanied by heavy fine-grained sediment loads being winnowed and transported away from these ridges and their parent sediments[17–22]. This kind of sediment distribution represents a distinctive coupled mud–sand sedimentary system on the coast and shelf of the ECS (Fig. 1). Such sedimentary patterns are common along the large river-dominated continental margins of the low–middle latitudes, which have shallow water depths, flat topography, and strong tides[23–27].

Sedimentological studies have amassed widespread evidence of the post-glacial sedimentary evolution of the ECS shelf as a result of

[1]Laoshan Laboratory, Qingdao, China. [2]Qingdao Institute of Marine Geology, Qingdao, China. [3]Estuary Research Center, Shimane University, Matsue, Japan. [4]College of Marine Geosciences, Ocean University of China, Qingdao, China. [5]Marine Geological Institute of Hainan Province, Haikou, China.
✉e-mail: liujian0550@vip.sina.com

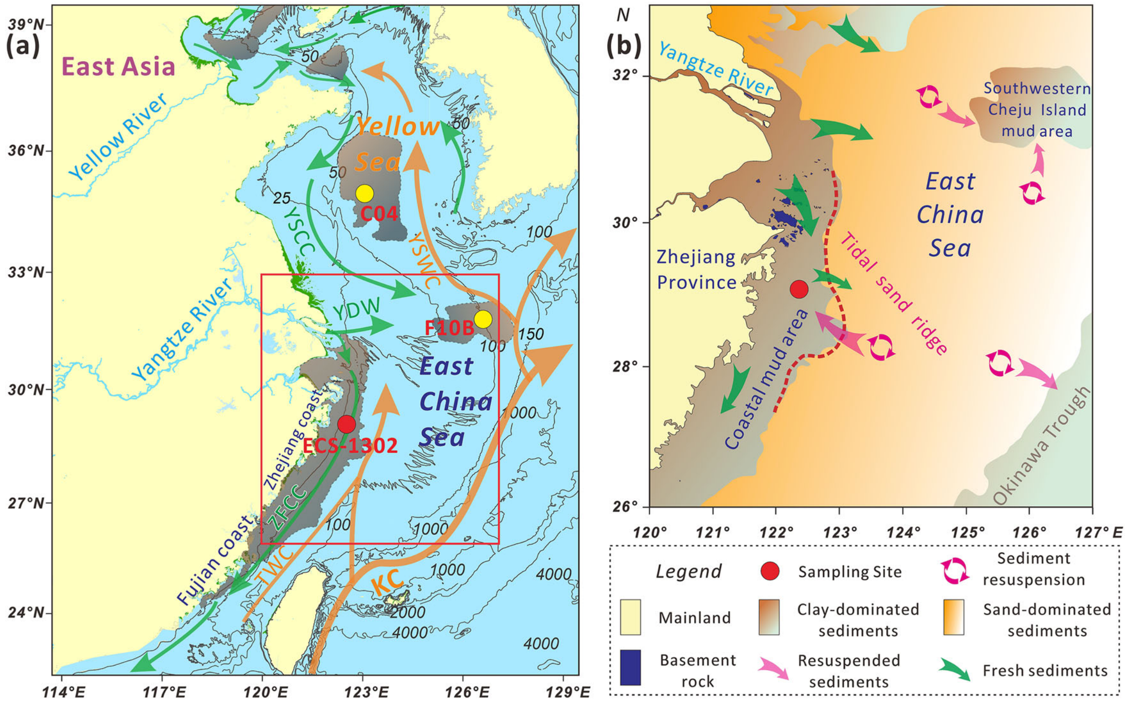


**Fig. 1 | General information on the study area. a** Schematic diagram illustrating the distribution of muddy deposits (modified after ref. 91) and circulation patterns (modified after ref. 92) in the eastern China marginal seas under the dominant influence of large rivers. Complex circulation systems trap fine-grained material contributed by large rivers within specific topographic settings, resulting in the formation of coastal muddy belts and shelf muddy patches (the gradient brown areas). The names of the circulation currents are indicated by acronyms. Green arrows represent cold coastal currents: Yellow Sea Coastal Current (YSCC), Yangtze Diluted Water (YDW), and Zhejiang–Fujian Coastal Current (ZFCC). Orange arrows represent warm currents: Yellow Sea Warm Current (YSWC), Taiwan Warm Current (TWC), and Kuroshio Current (KC). The red dot indicates the location of core ECS-1302 recovered from the Zhejiang coastal mud area, East China Sea, as used in this study. The yellow dots indicate the locations of other cores from previous studies that we used for comparison, including core F10B from the southwestern Cheju Island mud area and core C04 from the south Yellow Sea mud area[12]. The red solid box indicates the study area. **b** Sketch map showing the mud–sand coupled sedimentary system on the East China Sea shelf (modified after ref. 91). The dashed line shows the junction between the coastal mud area and the sand ridges (modified after ref. 29). Arrows indicate the direction of sediment transport.

environmental processes, including sea level change, wave action, tidal currents, shelf circulation, and episodic events[20,28,29]. Presently, the Yangtze River-derived sediments are sequestered mainly along the sediment dispersal system from the prodelta regions down to the coastal and inner-shelf areas[15], with a small amount of the sediments being transported seaward and deposited in the Okinawa Trough[30–32]. However, there is sequence stratigraphic evidence that sediments derived from older strata, which were deposited during the falling stages and/or low stands of sea level and buried on the middle and outer shelf, can be eroded and laterally advected shoreward during transgressions[29]. Shortly, the muddy belt functions not only as a distal repository for mud originating from the Yangtze River, but also receives fine-grained sediment that is reworked and transported shoreward from the sand ridges by strong tidal currents. As a result, the source-to-sink processes associated with sedimentary OC in the muddy belt could have been profoundly affected by shoreward sediment reworking. However, few studies have examined these processes. It is expected that combined bulk OC and biomarker parameters can provide valuable insights into the sedimentary sources and process-specific information associated with OC[33–36]. Crucially, by integrating organic geochemistry with visual observations of sedimentary strata, it is hoped to gain a more complete picture of the depositional processes that affect shallow marine environments[37].

In this study, we measured the bulk OC, as well as the associated isotopes ($^{13}$C and $^{14}$C) and molecular biomarkers (sterols, *n*-alkanes, long-chain alkyl diols, and tetraethers), preserved within sequential core ECS-1302 (29.02 °N, 122.37 °E; 38.2 m below sea level) collected from the Zhejiang coast of the ECS (Fig. 1). The depositional age of the core spanned approximately the last 14 kyr[29]. Our aim was to investigate the cyclic processes of sedimentary OC in the muddy belt from various sources within the deciphered sedimentary strata. Our data show marked sedimentary OC-$^{14}$C ages deviation from corresponding depositional ages and a decreasing proportion of terrestrial OC, which we attribute to the fact that the fine-grained terrestrial material reworked from the middle and outer shelf has contributed significantly to the accumulation of pre-aged OC on the muddy belt during the postglacial transgression, thus providing critical constraints on dual-directional cycles of sedimentary OC for large river- and tide-dominated marginal seas.

## Results

### Characteristics and temporal heterogeneity of sedimentary OC

The bulk OC and multi-biomarker records from the post-14 ka sedimentary succession of the uppermost 30.2 m of core ECS-1302 are shown in Fig. 2; Supplementary Table 1 and Supplementary Fig. 1, and the diverse sources of sedimentary OC from different depositional environments (i.e., three depositional units described in the following sections) are identified in Fig. 3.

**DU 3 (30.20–18.40 m; ca. 14–11 ka): central estuarine bay deposits.** The muddy central estuarine bay (Fig. 2a), which is characterized by a high mineral surface area and sedimentation rate (Fig. 4), is conducive to the adsorption and burial of OC[38]. Consequently, high levels of total OC (TOC) and terrestrial *n*-alkanes are observed in DU3 (Fig. 2). In addition, high sedimentation rates, a low sea level, and the close proximity of the study site to the coast most probably promoted increased OC burial efficiency during the last deglaciation[35]. Accordingly, our results indicate that the central estuarine bay deposits along the Zhejiang coastal area,

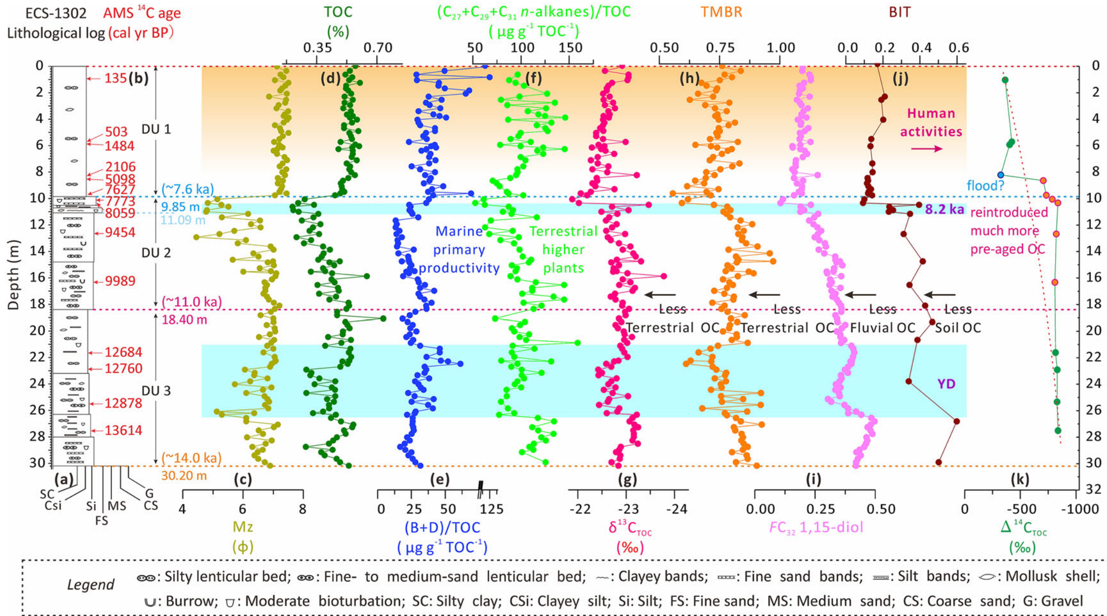


**Fig. 2 | Characteristics of, and proxies for, diverse sedimentary OC from core ECS-1302 in different depositional systems.** **a** Lithological log of core ECS-1302[29]. **b** Calibrated $^{14}$C ages and depositional units[29]. DU1: mud wedge deposits from coastal to shelf environments after the Mid-Holocene maximum flooding. DU2: tide-influenced coastal to shelf deposits covering the period around 11.0 to 7.6 ka. DU3: central estuarine bay deposits spanning the period around 14.0 to 11.0 ka. **c** Median grain size[29] (Mz). **d** TOC content. **e** (B + D)/TOC content, indicative of the abundance of marine primary productivity. **f** ($C_{27}+C_{29}+C_{31}$ *n*-alkanes)/TOC content, indicative of the abundance of terrestrial higher plants. **g** $δ^{13}C_{TOC}$ values, indicative of the contribution of terrestrial OC. **h** Terrestrial and Marine Biomarker Ratio (TMBR), indicative of the contribution of terrestrial OC. **i** $FC_{32}$ 1,15-diol[89], indicative of the contribution of fluvial OC. **j** Branched and Isoprenoid Tetraether (BIT), indicative of the contribution of soil OC. **k** $Δ^{14}C_{TOC}$ values from core ECS-1302. The red dotted line indicates the ideal decay curve of $Δ^{14}C_{TOC}$ in line with the depositional age under a stable sedimentary environment. The blue circle in DU1 indicates a suspected flooding layer. The rose red circles in DU1 and DU2 indicate that much more pre-aged OC has been reintroduced shoreward from the underlying old strata sediments. B + D: sum of brassicasterol and dinosterol. $C_{27}+C_{29}+C_{31}$ *n*-alkanes: sum of *n*-alkanes with 27, 29, and 31 carbon atoms. YD: Younger Dryas. The ice blue bands indicate cold episodes. The gradient orange band indicates the continuous increase in human activity over the last 2000 years.

spanning a time period of approximately 14.0–10.0 ka[29], acted as a highly efficient sink for terrestrial OC, with the largest proportion of terrestrial OC (avg. 51.2 ± 3.9%, $n = 52$) being recorded in DU3, compared with DU2 (avg. 51.0 ± 5.9%, $n = 40$) and DU1 (avg. 45.9 ± 4.2%, $n = 49$).

During the initial transgression, as the shoreline migrated landwards, increasing water depth enhanced the diffusion capacity of the water mass, leading to a high level of TOC and long-chain *n*-alkanes (Fig. 2), and a high contribution from terrestrial $C_3$ plants (Fig. 3c). Concurrently, reversely negative $δ^{13}C_{TOC}$ values (Fig. 2) and high TOC/TN ratios (Supplementary Table 1) indicate the greater contribution from terrestrial OC[38], and high values of TMBR, $FC_{32}$ 1,15-diol, and BIT (Fig. 2) indicate the enhanced contribution from terrestrial[39], fluvial[40], and soil[41] OC sources, to some extent, with a gradually increasing up-core trend. The humid YD cold event[42] led to a phased decrease in TOC, the terrestrial ($C_{27}+C_{29}+C_{31}$ *n*-alkanes)/TOC content derived from higher plants, and various terrestrial OC contributions under fierce hydrodynamic conditions, together with a coarsening sediment grain size (Fig. 2) and a pronounced increase in the sedimentation rate (Fig. 4), marine (B + D)/TOC content and marine OC contributions (Fig. 2). The termination of the YD was marked by the onset of Meltwater Pulse 1B, which triggered rapid sea level rise[28], leading to an increase in ($C_{27}+C_{29}+C_{31}$ *n*-alkanes)/TOC content and an increase in various terrestrial OC contributions but a stepwise decrease in (B + D)/TOC content (Fig. 2 and Supplementary Table 1).

**DU 2 (18.40–9.85 m; ca. 11–7.6 ka): tide-influenced coastal to shelf deposits**. During this period, the water depth continued to increase slowly, leading to the retreat of the coastline and the paleo-Yangtze mouth, accompanied by strengthened tidal dynamics and a decrease in the contemporary terrestrial sediment flux[29]. Correspondingly, the sediment grain size coarsened (Fig. 2c), while the terrestrial ($C_{27}+C_{29}+C_{31}$ *n*-alkanes)/TOC and marine (B + D)/TOC content, as well as the various terrestrial OC contributions, gradually decreased (Figs. 2e–j and 3c; Supplementary Table 1). An exception is evident in the contribution from the terrestrial higher plants and/or OC, inferred from the TMBR and TOC/TN ratios, which initially increased before declining (Fig. 2h and Supplementary Table 1). Nevertheless, the Zhejiang coast still experienced a period of unusually rapid deposition during which the site of core ECS-1302 received over 7 m of sediment in less than 3000 years (Figs. 2a and 4). This early Holocene succession is characterized by millimeter-scale interlaminations of dark gray clayey silt and silty sand to sandy silt, as well as weak to moderate bioturbation and well-developed tidal bedding[29]. In turn, although enhanced winnowing via resuspension can itself remove sedimentary OC and increase sedimentary OC decay rates[4], the dilution of massive lithogenic mineral components under the high sediment accumulation rates may have further contributed to the lower TOC values[34] that are evident in Fig. 2d.

Subsequently, a rapid sea level rise in response to the pre-8.2 ka sea level event[43] led to a pronounced landward retreat of the Yangtze River estuary, as far back as the Nanjing–Zhenjiang area[44], which generated the low values of TOC, TMBR, $FC_{32}$ 1,15-diol, and BIT values, as well as the positive $δ^{13}C_{TOC}$ (Fig. 2). These signatures coincide with the condensed section of relatively coarse-grained sediment at the top of DU 2 (9.85–11.09 m; Fig. 2a–c), which we interpret to be the result of sediment starvation (Fig. 4) during the maximum flooding stage[29].

**DU 1 (9.85–0 m; since 7.6 ka): inner-shelf mud wedge deposits**. The mud wedge is the twin of the Yangtze River delta and formed via the resuspension, transport, and re-deposition of Yangtze River-derived fine sediments[15]. Meanwhile, abundant nutrients were continuously being supplied into the study area during the sedimentary evolution of the mud

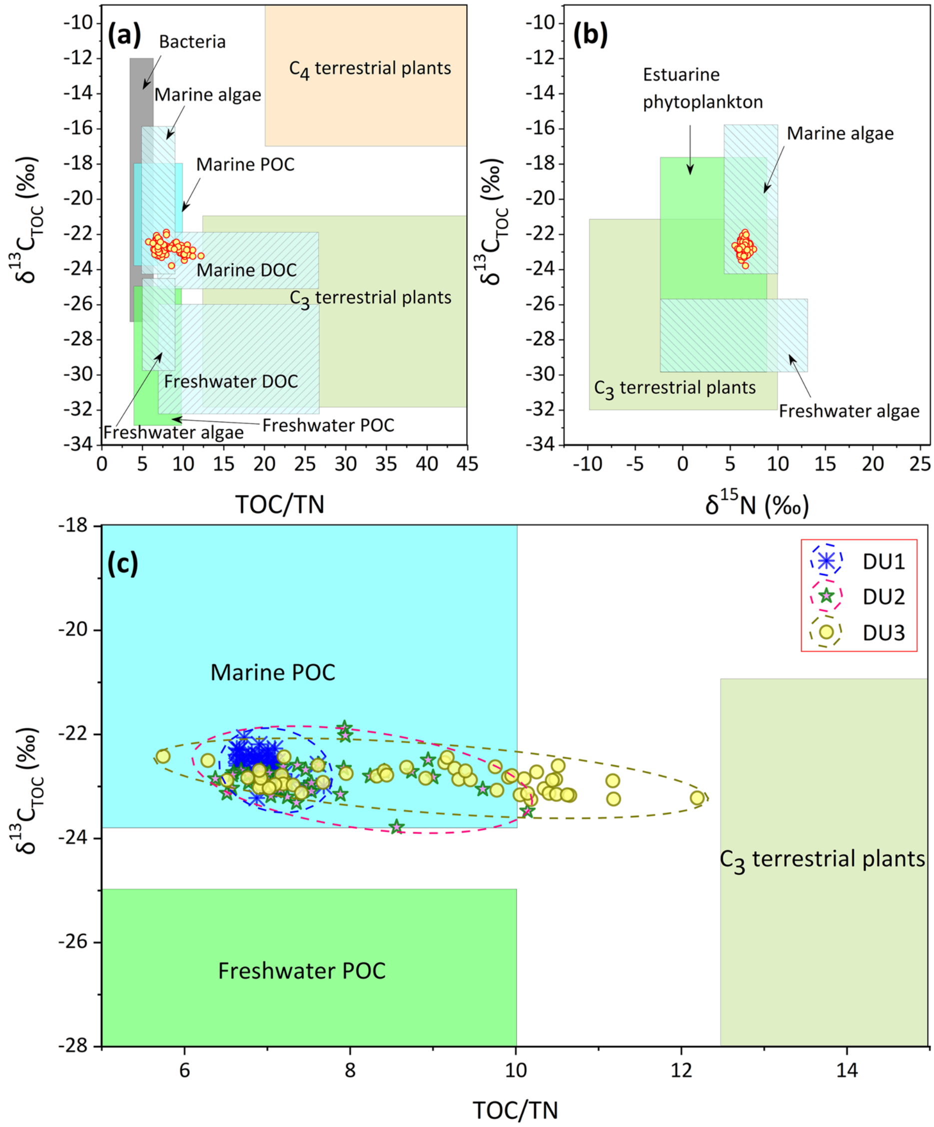


**Fig. 3 | OC source apportionment in the Zhejiang coast sediment record.** Cross-plot of $\delta^{13}C_{TOC}$ values and TOC/TN values (**a**) and $\delta^{13}C_{TOC}$ values and $\delta^{15}N$ values (**b**) for all samples ($n = 141$). Boxes mark the potential carbon sources[93,94]. The $C_3$ terrestrial plants are the dominant biomass in the central and East China[95]. **c** Close-up of (**a**) showing differences in values between three stratigraphic intervals defined in ref. 29, central estuarine bay deposits, tide-influenced coastal to shelf deposits, and mud wedge.

wedge[10]. The aforementioned factors modulated the TOC content, as well as the levels of terrestrial higher plants, fluvial and soil OC, and the contribution from various terrestrial OC sources with high and low values during this period (Fig. 2 and Supplementary Table 1). This pattern suggests that marine OC became the dominant contributor to sedimentary OC during the highstand period (Fig. 3c).

Notably, the TMBR, $FC_{32}$ 1,15-diol, and BIT values gradually increased over the last 2000 years and correspond to a negatively biased $\delta^{13}C_{TOC}$ and a relatively stable TOC content (Fig. 2), as well as a high sedimentation rate (Fig. 4). In particular, the (B + D)/TOC content, used as a proxy for marine primary productivity, peaked in recent centuries (Fig. 2). It is certain that human activities played a key role in this deviated natural deposit[10,11,15,45,46], particularly over recent decades[38].

### Sedimentary OC-$^{14}$C ages deviate anomalously from depositional ages

Logically, in relatively stable depositional systems with constant sediment sources, where contemporary OC from autochthonous plankton and allochthonous fresh biogenic components undergoes one-time deposition, the sedimentary OC-$^{14}$C ages would generally be expected to align with the corresponding planktonic foraminifera $^{14}$C ages and/or depositional ages[47,48]. Strontium (Sr) and neodymium (Nd) isotopic data from this study (Supplementary Table 2 and Supplementary Text 1) reveal distinct sediment source specificities over the past 14 ka, indicating a persistent dominance of Yangtze River-derived sediments (Supplementary Fig. 2). Intriguingly, markedly negative $\Delta^{14}C_{TOC}$ values during DU2 and early in DU1 indicate a decoupling from the predicted linear age–depth relationship (Fig. 2k and Supplementary Table 3).

## Discussion

### Negligible influence of petrogenic, marine, local river, and coastal OC reworking and bioturbation

The observed deviation in sedimentary OC-$^{14}$C ages (Fig. 2k), which is concurrent with a decreasing proportion of terrestrial OC (Fig. 2g–j), cannot be explained solely by the mixing of old terrestrial OC with contemporary marine OC[12]. This is because a lower terrestrial OC contribution would lead to a positive $\Delta^{14}C_{TOC}$ values and young OC age, vice versa, if assuming a constant terrestrial OC age[49].

Widespread carbonate-interlayered black shale in the upper reaches of the Yangtze River basin with less negative $\delta^{13}C_{TOC}$ (−21.5 ± 7‰) values[50] and containing radiocarbon-dead/$^{14}$C-depleted petrogenic OC[36] might import aged sedimentary OC. However, several lines of robust evidence from previous studies argue against a significant petrogenic influence. This is supported by: (i) the consistently low proportions of CaO and total inorganic carbon[45,51], (ii) the abundant presence of shale, igneous fragments and their weathering products without notable decrease[52], (iii) the relatively

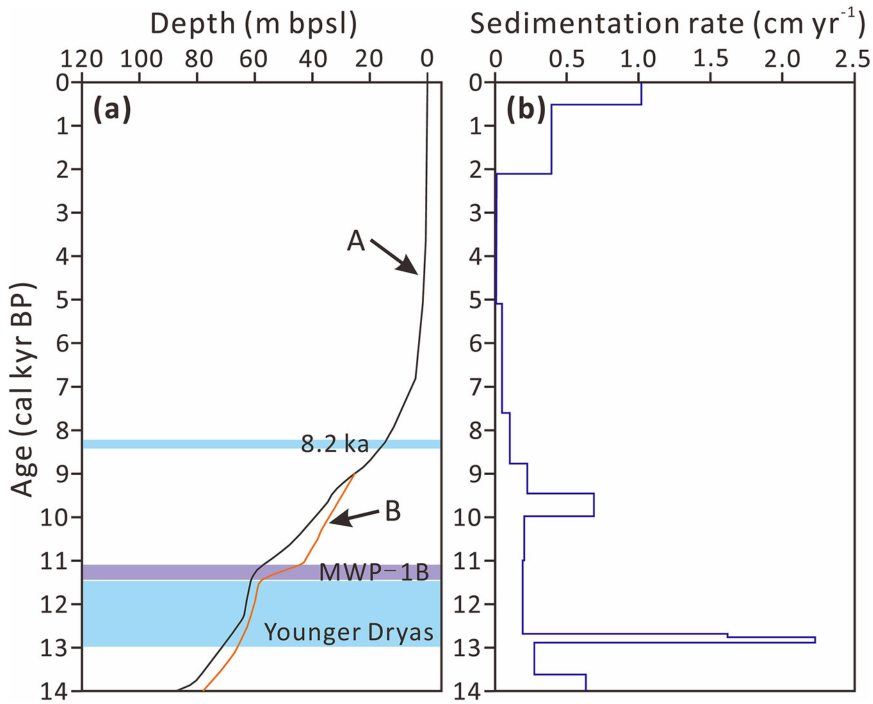


**Fig. 4 | Local sedimentation rates corresponding to sea level changes.** The post-glacial sea level curve (**a**) and sedimentation rate of core ECS-1302 (**b**). Black line A represents the global averaged ice volume equivalent sea level curve since 14 ka[96] and orange line B represents the Barbados U–Th-dated sea level curve between 13.9 and 9 ka[97]. The horizontal bands of various colors indicate the major climatic events in the following intervals: the Younger Dryas cold period (pale blue band; 12.85 to 11.65 ka)[98], MWP-1B (purple band; 11.45 to 11.1 ka)[97], and the 8.2 ka cooling event (pale blue band; 8.34 to 8.18 ka)[99].

stable $\delta^{13}C_{TOC}$ values in the Yangtze River estuary[46]. Furthermore, (iv) sediment inputs remained stable during these depositional periods[28,29] despite the complicated dry (11.5–9.6 ka) to wet and then dry (7.5–3 ka) climatic conditions in the source regions[53], not to mention (v) the enhanced oxidation of petrogenic OC[2] during longer sediment transport in the Yangtze River catchment[54]. The carbon preference index of high-molecular-weight *n*-alkanes ($CPI_{alk\ 25-33}$) in core ECS-1302 during these depositional periods provides further support for this inference. The observed values, ranging from 3.2 to 5.9 (avg. 4.7 ± 0.9, $n = 14$; Supplementary Table 3), significantly exceed the diagnostic values of petrogenic material (~1), pointing to the dominance of fresh OC from immature deposits (ref. 35 and references therein).

Under a lowering sea level, cross-shelf downslope lateral transport of marine OC derived from seaward sediment reworking can result in bulk OC aging[55]. The coeval decrease in terrestrial OC contribution (Fig. 2g–j), rising local sea level[28], and weakening East Asian winter monsoon[56] during the early-middle Holocene rule out the reworking of marine OC by lateral seaward transport as the cause of the observed aging trend.

During the early Holocene transgression, sediment input from smaller local rivers or from coastal erosion might have maintained the sedimentary evolution of the ECS inner shelf[29], and could have introduced $^{13}C$- and $^{14}C$-depleted aged biospheric OC or fossil fuel-related OC. However, evidence of unusually rapid deposition in the adjacent Sanmen Bay[57], and an increased contribution of Yangtze-derived sediments in the modern Mulanxi estuary[58] between about 11.5 and 7.7 ka, suggest that the shelf supplied quite astonishing Yangtze River sediments to the near-coast area. Furthermore, considering the negligible sediment flux from small rivers when compared with that from the Yangtze River[58], and the absence of coastal progradation in the facies architecture of the study area[29], the above evidence excludes the possibility that smaller local rivers and coastal erosion were the major sediment sources during this stage.

The supply of young carbon from bioturbation (i.e., vertical mixing of the sediment itself via burrowing, excretion from living organisms, and dead organisms) may also have affected our OC $^{14}C$ ages[59]. In this case, the common moderate bioturbation, and vertical or oblique burrows during DU2 (Fig. 2a), coupled with an increase in the proportion of the younger marine OC (Fig. 2g–j), should theoretically have resulted in much younger $^{14}C_{TOC}$ ages. However, the opposite occurred, which suggests a much more abundant supply of aged OC. Conversely, bioturbation and bioirrigation can enhance oxygen penetration, which facilitates the more efficient decomposition of particulate OC and the removal of younger fractions[60]. Given that moderate bioturbation and relatively high sedimentation rates are evident in both DU3 and DU2, and that bioturbation does not increase over time[29], its net effect on OC aging is likely to have been minor[61].

Collectively, our analysis indicates that a complex carbon recycling process operates within the study area.

## Sedimentary OC recycling from shelf to coast

The apparent initial age of TOC ($AIR_{TOC}$) at the time of deposition is a key parameter for tracing OC sources and cycling dynamics[12,62,63]. During the deposition of DU3, which acted as a major sink for fluvial particulate OC (Fig. 5a), the average $AIR_{TOC}$ value was 3073 ± 280 yr (Supplementary Fig. 3). This aligns with the millennial-scale $^{14}C$ age (~2870 yr) obtained for the surface mixed layer of global continental margin sediments, particularly the modern Yangtze River estuary and adjacent seas[7]. The latter age reflects the complex aging, degradation, and sorting processes of terrestrial biospheric and petrogenic OC during transfer from source to shelf, combined with marine biospheric OC inputs[4,36,49,60].

During the transgression from the early MIS 1 transgressive ravinement surface (TRS) to the Middle Holocene maximum flooding period (DU2; Fig. 5b), the ECS shelf was shallow and experienced strong tidal currents[29]. Tidal and/or storm-driven currents resuspended shelf deposits, reworking estuary-mouth complexes and forming the coarsening-upward DU2 unit with abundant tidal beddings and scattered shell fragments[29]. Concurrently, large-scale tidal sand ridges developed and migrated shoreward on the middle and outer shelf under optimal water depths of ~20–30 m during the early Holocene deceleration in the rate of sea level rise[18,20,21,29]. These westward-migrating sand ridges eroded the underlying DU2 deposits, contributing to an aggradational to retrogradational stacking pattern along the Zhejiang coast[29]. Meanwhile, the tidal-triggered "bottom-up carbon pump"[64] resuspended and transported pre-aged OC, initially stored in the DU3 estuary-mouth complex on the present middle-to-outer shelf, back into the inner shelf along high tide rather than low tide. Indeed, mixing and redeposition of this pre-aged OC with contemporaneous fresh

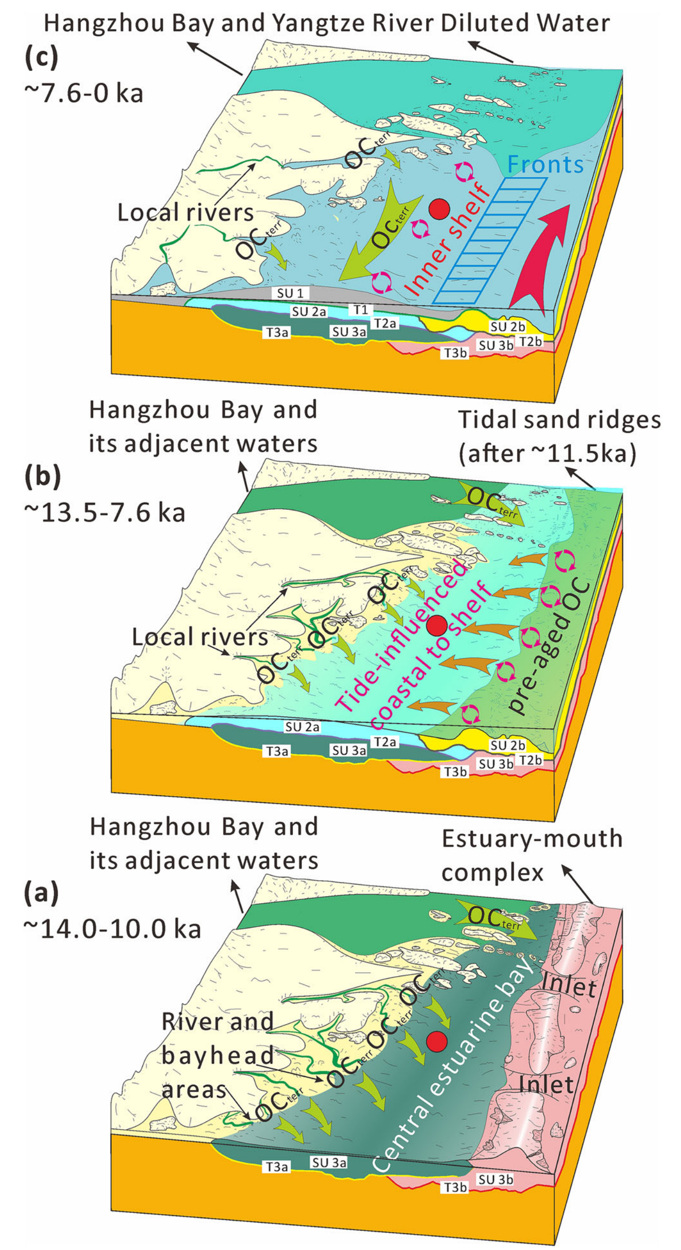


**Fig. 5 | Effects of localized sedimentary evolution on the sedimentary OC cycle.** **a** Large amounts of terrestrial sediment carried seaward by rivers enabled the central estuarine bay to act as a terrestrial carbon sink and the associated formation of the estuary-mouth complex during DU3. **b** The reworking and subsequent advection of old strata sediments allowed for the reintroduction of old OC, which had been sequestered in middle and outer shelf sediments for thousands of years, into the contemporary carbon cycle of the inner shelf, especially during DU2. **c** The permanent fronts[100], comprising the coastal current (light green arrow) and the Kuroshio intrusion current (red arrow), effectively prevented the interaction and transport of substances between the nearshore and the open sea during DU1. OC$_{terr}$ refers to terrestrial OC. The red dot indicates the location of core ECS-1302. Seismic units/subunits (SU 1, SU 2a, SU 2b, SU 3a, and SU 3b) and seismic surfaces between the seismic units/subunits (T1, T2a, T2b, T3a, and T3b) are described in detail by ref. 29.

terrestrial OC led to significant apparent OC aging (Supplementary Fig. 3). Post-depositional aging intensified with the progressive shoreward sediment reworking, peaking to ~7213 yr of AIR$_{TOC}$ in the condensed section (Supplementary Fig. 3)[29] where inputs of fresh, younger terrigenous OC were minimal. Our TMBR and TOC/TN values reflected the shoreward reintroducing of pre-aged OC during the DU2 stage, exhibiting unusual peaks (Fig. 2h; Supplementary Table 1), which was related to the increase in the contribution from terrestrial higher plants and/or OC[38]. In contrast, this pattern was not captured by $FC_{32}$ 1,15-diol or BIT, which can originate from the preferential degradation of younger and more labile components of fluvially transported diols, tetraethers, and sterols compared with *n*-alkanes[65,66]. It is worth highlighting that the radiocarbon values of the aged terrestrial material might be even more $^{14}$C-depleted than the measured bulk $^{14}$C values due to dilution by fresh marine phytoplankton[4]. Future studies employing compound-specific $^{14}$C analysis, such as $^{14}$C-lignin or $^{14}$C-plant wax, could help to further reduce these uncertainties[35].

During the inner-shelf mud wedge depositional stage, the frontal blocking effect formed by the coastal current and the Kuroshio branch current (Supplementary Fig. 4a) prevailed along the ECS coast, preventing material exchange between the inner shelf and the middle to outer shelf[67]. However, during the early DU1 stage (Fig. 2k), when the intensity of the East Asian winter monsoon was weak[56], and the intensity of the Kuroshio Current intrusion onto the inner shelf was weak due to the influence of topography and other driving forces[68], the frontal effect was therefore weakened in our study area, resulting in minimal barrier impact on the sediments. Thus, there were still more pronounced pre-aged OC, with an average AIR$_{TOC}$ value exceeding 3000 yr (Supplementary Fig. 3), resulting from minor middle to outer shelf sediments being transferred into our study area under the strong tidal influence. Additionally, this associated mechanism resulted in the almost complete absence of sedimentation in the tidal sand ridge area near station DH03 (Supplementary Fig. 4b) on the ECS middle to outer shelf during this period[21]. From the late DU1 stage (~2 ka; Fig. 5c), the frontal effect was strengthened by the intensified East Asian winter monsoon and Kuroshio intrusion[56,68], effectively blocking shoreward transport of middle to outer shelf sediments. Although local near-bed current velocities of up to 0.55 m/s can move unconsolidated sand particles, the reworked and advected sediments of the active tidal sand ridges near our study area are still deposited mainly on the middle to outer shelf, generating an irregular chronological sequence[21]. Correspondingly, the AIR$_{TOC}$ values on the inner shelf (Supplementary Fig. 3) are again consistent with the observed variable ranges for millennial storage of biospheric carbon in continental reservoirs prior to delivery to marginal sea sediments (~3.5 ± 0.5 ka), which can be attributed to stable tectonics, moderate erosion rates and temperate climate in the Yangtze River basin[7,69]. Given that the contemporary fluvial particulate OC composition is dominated by young plant and soil materials[49], and the relatively coarse sediment components on the ECS shelf are composed mainly of old OC[70], we can confidently infer that the tidal sand ridge region may still supply a certain proportion of pre-aged coarse particle components to the inner shelf even today under frontal instability conditions.

It is worth noting that the $\Delta^{14}C_{TOC}$ value exhibits an anomalous positive bias at a depth of 8.22 m (Fig. 2k), with a young AIR$_{TOC}$ value of approximately 953 yr (Supplementary Fig. 3), corresponding to the depositional age of 2079 cal yr BP. This coincides with a more positive $\delta^{13}C_{TOC}$ and higher $FC_{32}$ 1,15-diol values (Fig. 2g, i), coherently revealing a large increase in the contemporary fluvial terrigenous OC contribution, which can be attributed to an extreme flood event in the sediment source basin[49].

To summarize, the ECS inner shelf exhibits a characteristic dual-directional sedimentary OC cycle pattern, involving seaward cross-shelf/alongshore dispersal and retrograde (shoreward) cross-shelf transport (Figs. 1b and 5).

## Implications for regional sedimentary evolution and global carbon cycle

A comparable sedimentary OC aging trend is observed in the Southwestern Cheju Island Mud (SWCIM) at site F10B (Supplementary Fig. 4b)[14]. The SWCIM overlays the Late-Pleistocene residual sand on the northern outer shelf of the ECS and trapped abundance of high-energy tidally reworked sediments during the early Holocene[71]. The onset of marked sedimentary OC aging in the SWCIM corresponds exactly with the timing of formation of the adjacent Yangtze Shoal sand sheet (Supplementary Fig. 4b) in response to post-glacial transgression of the paleo-Yangtze River estuary[72]. Accompanying the shelf circulation (Supplementary Fig. 4a), the tidal residual currents in the bottom turbid layer should have jointly transported a great deal of pre-aged and resuspended sediment derived from the Yangtze Shoal sand sheet and its adjacent tidal sand ridge on the ECS middle to outer shelf into the SWCIM (Supplementary Fig. 4b). These currents flow in the same directions as the Yellow Sea Coastal Current (YSCC), the Taiwan Warm Current (TWC)/Kuroshio intrusion current off the Yangtze River mouth, and the Yellow Sea Warm Current (YSWC), particularly during the winter-half-year[73]. A similar sediment transport pattern has been reported in the North Sea, where areas with tidal sand ridges, sand waves, tunnel valleys, iceberg grooves, and other (post-) glacial relict structures are present[74]. Specifically, sediment reworking flows from offshore and along the coast provide a major supply to the localized mud depocenter in the German Bight, while contemporary fluvial sediment outflows contribute only marginally[75]. In contrast, the marked aging of the sedimentary OC during the transgression of the early Holocene is missing from sediments at site C04 (Supplementary Fig. 4b) in the central southern Yellow Sea mud[12], where the tidal bottom stress was weak[20], and the site was distant from tidal depositions[18]. Hereby, we properly propose that such processes, previously unrecognized, may be prevalent in the shallow and flat marginal seas adjoining active tidal sand ridges and sheets, where intense sediment reworking from the tidal sand ridges or sheets exerts a widespread and non-negligible influence on sedimentary OC aging.

Especially, strong tidal-driven geostrophic currents can have a significant impact on sediment dynamics on the ECS shelf; i.e., increased bottom shear stress triggered massive shoreward sediment resuspension and redistribution in nearshore shallow regions and elevated sediment depositional rates on the present inner shelf during the early Holocene. Consequently, our study presents compelling direct evidence that substantial amounts of reworked sediment could have supported the rapid deposition on the ECS inner shelf through the early Holocene. During this period, direct riverine sediment outflow from the Yangtze River played only a minor role in the distal sedimentary system because of the insufficient precipitation driven by the weak hydrometeorological forcing (e.g., the interaction of the El Niño–Southern Oscillation[76] and the East Asian summer monsoon[77]), and the heavy sediment consumption in response to early paleo-Yangtze River estuary fillings[78], termed as "Holocene rapid deposition conundrum". Additionally, we confirmedly propose that in the context of the sharp reduction in sediment input derived from the Yangtze River due to major human projects, apart from the erosion and supply of the estuary, coast, and subaqueous delta[10], the sediment reworking of offshore old strata will become more pronounced in terms of the maintenance of inner shelf muddy deposits in the future when the intensity of the ECS coastal fronts decreases in response to the weakening East Asian winter monsoon[79] and the intensifying Kuroshio under a warming climate[80].

This newly identified pattern clearly differs from previous interpretations that described how the pool of old OC was mainly eroded and laterally advected through gravity flows seaward in the pan-Arctic shelf area with extensive permafrost and sea-ice cover[35,66,81], and the continental slopes with cliffy topography[8,20,32,55,82], as well as in submarine canyons incising the continental shelf[62,83]. Given the scale of the tidal deposits on the present-day middle and outer shelves at the glaciation[23,25–28,84], future paleoclimate modeling of the global carbon cycle should include the pre-aged sedimentary OC recycling during deglaciation. Specifically, in the future, it would be valuable to improve the precision of the assessment of geological OC sinks by effectively eliminating the pre-aged sedimentary OC from the reworked old strata when calculating the OC burial flux over a longer timescale. However, quantifying the contribution of reworked OC remains challenging because tidal deposits might be the product of a periodic glacial–interglacial cycle synchronized with the highly dynamic recurring erosive transportation of sediment[21], which compromises the use of the repetitive aged paleodeposit-derived OC as a distinct endmember. Furthermore, the long-term contributions of this process at the global scale to the atmospheric $CO_2$ concentrations rise[85] and radiocarbon content decrease[86] remain poorly understood, meaning that further investigation is needed.

## Methods

### Core location and description

The sediment core ECS-1302 (29.02°N, 122.37°E; 38.2 m below sea level; 60.90 m long) was drilled on the inner shelf mud wedge of the ECS (Fig. 1) in 2013 with the vessel Kan 407. For this study, subsamples from the top 30.2 m of core ECS-1302 were collected at intervals of 10–20 cm. The depositional ages of the core sediments covering approximately the past 14,000 calibrated radiocarbon years before 1950 CE (cal yr BP; or using "ka" in place of "cal kyr BP") were determined using accelerator mass spectroscopy (AMS) $^{14}C$ data from mixed benthic foraminifera and/or shell debris, and have been reported by Liu et al.[29]. In brief, the raw radiocarbon dates were calibrated to calendar ages (i.e., cal yr BP) using the Calib 8.2 age calibration program (http://calib.org/calib/), in conjunction with the Marine 20 radiocarbon age calibration curve and a regional marine reservoir age of $\Delta R = -66 \pm 30$ years[29]. Through linear interpolation between age-stratigraphic control points and linear extrapolation, the depositional age of each sedimentary stratum was calculated.

Liu et al.[29] elucidated the Late Pleistocene to Holocene facies architecture and sedimentary history of the Zhejiang coast using an integrated analysis of high-resolution shallow seismic and core data, combined with previous research findings. In our study area, since about 14 ka, as sea level increased, the coarse-grained (sandy) deposits associated with an estuary-mouth complex (i.e., flood-tidal deltas, tidal inlets, washovers, and/or barrier beaches) began to develop in the eastern part of the area, and fine-grained (muddy) deposits of the central estuarine bay (DU3) began to develop in the western part of the area where core ECS-1302 was recovered. A TRS was formed by erosional shoreface retreat under the rising sea level of the early MIS 1 from about 13.5 ka in the southeastern part of the study area to about 10.0 ka in the area close to the shore, and this separated the underlying estuarine deposits from the overlying coastal to shelf deposits (DU2). Tidal sand ridges on the present-day middle shelf were formed at about 11.5 ka and have been completely or largely eroded by the underlying tide-influenced coastal to shelf deposits since then. The tidally influenced coastal to shelf depositional unit in core ECS-1302 formed during the period of slowly increasing sea level between 11.0 and 7.6 ka. The pre-8.2 ka sea level jump contributed to the formation of the maximum flooding surface, followed by the formation of the highstand system tract, and the modern marine circulation in the ECS essentially formed after that. The postglacial sea level rise peaked around 7.6 ka in the study area, and then a mud wedge (DU1), extending from the Yangtze Estuary southward off the Zhejiang and Fujian coasts into the Taiwan Strait, was formed under the combined influence of the modern marine circulation and inherited topography and geomorphology.

### TOC, TN, $\delta^{13}C_{TOC}$, $\delta^{15}N$, and $^{14}C$ analysis

Measurements of bulk organic matter parameters were performed on freeze-dried and homogenized bulk sediment at the Qingdao Institute of Marine Geology and the Center for Isotope Geochemistry and Geochronology of Laoshan Laboratory, Qingdao, China. Briefly, ~0.5 g subsamples were acidified using 1 M HCl to remove carbonate, rinsed repeatedly with Milli-Q water until the pH reached neutrality, and then freeze-dried for 48 h. The analytical procedures were conducted using an element analyzer and a Thermo 253 Plus Isotope Ratio Mass Spectrometer (IRMS). Control standards were run alongside the samples to correct the $\delta^{13}C_{TOC}$ and $\delta^{15}N$ values.

For $^{14}C$ analysis, sediment aliquots were weighed into silver cups and repeatedly acidified with 1 M HCl to remove carbonate, and were then measured using AMS after graphitization of the sample $CO_2$. The $^{14}C$ values of TOC are expressed as the fraction of modern carbon (Fm; relative to atmospheric $^{14}C$ abundance in 1950 CE) and corrected for carbon isotopic fractionation that occurred during sample processing. The measured

$Fm_{TOC}$ values and their associated uncertainties are provided in Supplementary Table 3.

### Estimates of terrestrial and marine OC fractions

A Bayesian two-endmember mixing approach, employing the $\delta^{13}C_{TOC}$ values, was used to estimate the proportional contributions of terrestrial OC ($OC_{terr}$) and marine OC ($OC_{mar}$) in the various depositional units. $\delta^{13}C_{TOC}$ values of −25.6‰ and −20.0‰ were assigned to the terrestrial OC and marine OC endmembers[38], respectively. The fractions of $OC_{terr}$ ($f_{terr}$) and $OC_{mar}$ ($f_{mar}$) in our core sediments can be estimated as follow:

$$\delta^{13}OC_{mar} \times f_{mar} + \delta^{13}OC_{terr} \times f_{terr} = \delta^{13}OC_{sample} \quad (1)$$

$$f_{mar} + f_{terr} = 1 \quad (2)$$

### Calculation of apparent initial radiocarbon ages

The age of OC at the time of its burial not only serves as a tracer of OC sources with diverse ages, but also provides a window into the dynamics of OC recycling and transfer between the various OC surface reservoirs[12]. Soulet et al.[63] defined $F^{14}R_{x-y}$ as a reservoir's "relative enrichment" of $^{14}C$. The sedimentary OC-$^{14}C$ age offset, also known as the apparent initial radiocarbon age ($AIR_{TOC}$) of the relatively $^{14}C$-depleted reservoir TOC, between TOC and the contemporaneous atmosphere (TOC-atm) at any deposition time is calculated to eliminate the reservoir effect and decay effect of down-core sample radiocarbon content. The parameters are calculated as follows:

$$F^{14}R_{x--y} = Fm_x / Fm_y \quad (3)$$

$$AIR_{TOC} = \text{-}8033 \times \ln(F^{14}R_{x--y}) \quad (4)$$

where y is atmosphere and x represents the TOC reservoir. By convention, $F^{14}R$ is dimensionless and takes a value from 0 to 1 by assigning the more commonly enriched reservoir (y) as the denominator. Thus, we selected the atmosphere as the reservoir (y) because under natural circumstances (i.e., the pre-nuclear era) the atmosphere was always the most uniform and $^{14}C$-enriched global carbon reservoir relative to all other carbon reservoirs[63], and atmospheric $CO_2$ radiocarbon isotope values ($Fm_{atm}$) are well-constrained for the past 14,000 calendar years[86].

### Lipid biomarker analysis

Lipid biomarker analysis was performed at the Qingdao Institute of Marine Geology. Freeze-dried, homogenized, and powdered samples (~8 g) were extracted twice using a mixture of dichloromethane (DCM) and methanol (MeOH; 3:1, v/v) in an accelerated solvent extractor (DIONEX ASE 200) at 110 °C after adding a known amount of *n*-tetracosane-$d_{50}$ (*n*-$C_{24}D_{50}$), *n*-nonadecanol, and $C_{46}$ glycerol trialkyl glycerol tetraether ($C_{46}$ GTGT) as internal standards. Sulfur in an aliquot of the total lipid extracts was removed by the addition of activated copper overnight. Saponification was performed by reaction at 70 °C for 30 min after the addition of a solution of 0.5 N KOH in MeOH to dried extracts. Neutral lipids were partitioned with 12 mL hexane, and were further separated by silica-gel chromatography using 8 mL hexane and 12 mL DCM:MeOH (95:5, v/v) to elute the apolar and polar fractions, respectively. The polar lipids were dried under a gentle stream of nitrogen and derivatized at 70 °C for 1 h with N,O-bis-(trimethylsilyl)trifluoroacetamide (BSTFA). To measure glycerol dialkyl glycerol tetraethers (GDGTs), part polar fractions were dissolved in hexane/isopropanol (99:1, v/v) and filtered through 0.45-μm PTFE syringe filters.

The lipid fractions, including alkanes, sterols, and long-chain alkyl diols, were redissolved in a known amount of hexane and identified by gas chromatography–mass spectrometry (GC–MS; Agilent 7890A/5975C) using a DB-5MS UI capillary column (30 m × 0.25 mm × 0.25 μm). Using helium as the carrier gas at 1.0 mL/min, 1 μL of sample was injected at 280 °C. The program for the apolar fractions (i.e., alkanes) started at 60 °C, was held for 1 min, increased to 310 °C at 5 °C/min, and held for 5 min. The program for the polar derivatives (i.e., sterols and diols) started at 80 °C, was held for 1 min, increased to 200 °C at 25 °C/min, increased to 300 °C at 4 °C/min, and then held for 15 min. The electron ionization source was set at 230 °C and 70 eV. Scanning was undertaken between m/z ranges of 50–600 Daltons. Individual components were identified with reference to retention times, previous literature, and the NIST mass spectrometry library. The long-chain alkyl diols were quantified using single ion monitoring (SIM) of the masses m/z 299 ($C_{28:1}$ and $C_{28}$ 1,14-diols), 313 ($C_{28}$ 1,13-diol and $C_{30}$ 1,15-diol), 327 ($C_{30:1}$ and $C_{30}$ 1,14-diols), and 341 ($C_{30}$ 1,13-diol and $C_{32}$ 1,15-diol), which represent characteristic fragment ions of the relevant long-chain alkyl diols[87] and contribute similarly to the total ion current of these lipids. The content of the long-chain alkyl diols could not be calculated due to the lack of standards, but their fractional abundances were calculated from integrated relevant peaks in the obtained mass chromatograms. A procedural blank, which was run in sequence with our sediment samples, presented no significant background interference. The GDGTs redissolved in hexane were analyzed using an Agilent 1200 series HPLC coupled to an Agilent 6130 quadrupole mass selective detector following the method of Wang et al.[88]. Selected ion monitoring mode was used to scan for mass/charge ratios of 1,292 (Crenarchaeol), 1,050 (GDGT-I), 1,036 (GDGT-II), 1,022 (GDGT-III), and 744 ($C_{46}$ GTGT).

### Estimates of terrestrial/higher plants, fluvial, and soil OC fractions, and carbon thermal maturity

The input of terrestrial/higher plants-derived OC into the ECS can be traced using the Terrestrial and Marine Biomarker Ratio (TMBR) index, because the total amount of $C_{27} + C_{29} + C_{31}$ *n*-alkanes is a reliable terrestrial OC indicator, whereas the algal biomarkers brassicasterol and dinosterol are reliable marine OC indicators[39]. TMBR is calculated as follows:

$$TMBR = (C_{27} + C_{29} + C_{31})/(C_{27} + C_{29} + C_{31} + B + D) \quad (5)$$

where $C_x$ represents the concentration of the corresponding *n*-alkanes, and B and D represent brassicasterol and dinosterol, respectively.

The input of fluvially produced OC into the ECS can be traced using the fractional abundance of $C_{32}$ 1,15-diol ($FC_{32}$ 1,15-diol), which is produced predominantly in freshwater, relative to that of the other 1,13- and 1,15 long-chain diols that have a marine origin[40]:

$$FC_{32}1,15-\text{diol} = [C_{32}1,15]/([C_{28}1,13] + [C_{30}1,13] + [C_{30}1,15] + [C_{32}1,15]) \quad (6)$$

where $[C_x]$ represents the fractional abundance of the corresponding diols. The detailed long-chain diols data have been reported by Chen et al.[89].

The input of soil-derived OC into the ECS can be traced using the Branched and Isoprenoid Tetraether (BIT) index, accepting the presumed soil origin of branched GDGTs relative to that of crenarchaeol, an isoprenoid GDGT that is exclusively produced by *Thaumarchaeota*[41]:

$$BIT = (GDGT-I + GDGT-II + GDGT-III)/(GDGT-I + GDGT-II + GDGT-III + Crenarchaeol) \quad (7)$$

The carbon preference index of *n*-alkanes ($CPI_{alk\ 25-33}$) was calculated to indicate carbon thermal maturity[90], as follows:

$$CPI_{alk25--33} = [(C_{25} + C_{27} + C_{29} + C_{31} + C_{33})/(C_{24} + C_{26} + C_{28} + C_{30} + C_{32}) + (C_{25} + C_{27} + C_{29} + C_{31} + C_{33})/(C_{26} + C_{28} + C_{30} + C_{32} + C_{34})]/2 \quad (8)$$

where $C_x$ represents the concentration of the corresponding *n*-alkanes. A $CPI_{alk}$ value of >3 indicates significant contributions of fresh OC from immature deposits, whereas a value of ~1 indicates the dominance of thermally mature OC (ref. 35 and references therein).

## Data availability

The data generated in this study are provided in the Supplementary Information and will be made available as open access in electronic form at the Mendeley Data repository at https://data.mendeley.com/ (https://doi.org/10.17632/mjkj29hnzh.1).

Received: 5 December 2025; Accepted: 8 May 2026;
Published online: 20 May 2026

## References

1. Bauer, J. E. et al. The changing carbon cycle of the coastal ocean. *Nature* **504**, 61–70 (2013).
2. Galy, V., Peucker-Ehrenbrink, B. & Eglinton, T. Global carbon export from the terrestrial biosphere controlled by erosion. *Nature* **521**, 204–207 (2015).
3. Ausín, B. et al. Sources and fate of sedimentary organic matter in the Western Mediterranean Sea. *Glob. Biogeochem. Cycles* **37**, e2023GB007695 (2023).
4. Bao, R. et al. Organic carbon aging during across-shelf transport. *Geophys. Res. Lett.* **45**, 8425–8434 (2018).
5. Canuel, E. A. & Hardison, A. K. Sources, ages, and alteration of organic matter in estuaries. *Annu. Rev. Mar. Sci.* **8**, 409–434 (2016).
6. Wang, C. et al. Global patterns of organic carbon transfer and accumulation across the land–ocean continuum constrained by radiocarbon data. *Nat. Geosci.* **17**, 778–786 (2024).
7. Yu, M. et al. Apparent aging and rejuvenation of terrestrial organic carbon along the river-estuary-coastal ocean continuum. *Geophys. Res. Lett.* **51**, e2023GL107855 (2024).
8. Tesi, T. et al. Reexposure and advection of $^{14}$C-depleted organic carbon from old deposits at the upper continental slope. *Glob. Biogeochem. Cycles* **24**, GB4002 (2010).
9. Liu, S. et al. Intensification of the East Asian winter monsoon resulted in greater preservation of terrestrial organic carbon on the inner shelf of the East China Sea since the last 1400 years. *Palaeogeogr. Palaeoclimatol. Palaeoecol.* **615**, 111454 (2023).
10. Su, J., Wu, Y. & Fan, D. Holocene to anthropocene burial of organic carbon in the Yangtze delta. *Geosci. Front.* **16**, 102162 (2025).
11. Zhang, M. et al. Fate of terrigenous organic carbon within shelf sediments from the East China Sea controlled by sea-level and climatic changes since the last deglaciation. *Palaeogeogr. Palaeoclimatol. Palaeoecol.* **650**, 112386 (2024).
12. Chen, M., Li, D. W., Zhang, H., Wang, Z. & Zhao, M. Distinct variations and mechanisms for terrestrial OC $^{14}$C-ages in the Eastern China marginal sea sediments since the last deglaciation. *Quat. Sci. Rev.* **315**, 108235 (2023).
13. Diesing, M. et al. Glacial troughs as centres of organic carbon accumulation on the Norwegian continental margin. *Commun. Earth Environ.* **5**, 327 (2024).
14. Zhang, H. et al. Hydrodynamic processes and source changes caused elevated $^{14}$C ages of organic carbon in the East China Sea over the last 14.3 kyr. *Geochim. Cosmochim. Acta* **304**, 347–363 (2021).
15. Liu, J. P. et al. Flux and fate of Yangtze River sediment delivered to the East China Sea. *Geomorphology* **85**, 208–224 (2007).
16. Shi, X. et al. Distribution, burial fluxes and carbon sink effect of sedimentary organic carbon in the eastern China seas. *Sci. China Earth Sci.* **67**, 3062–3082 (2024).
17. Chen, Z., Saito, Y., Hori, K., Zhao, Y. & Kitamura, A. Early Holocene mud-ridge formation in the Yangtze offshore, China: a tidal-controlled estuarine pattern and sea-level implications. *Mar. Geol.* **198**, 245–257 (2003).
18. Liu, Z. et al. Tidal deposition systems of China's continental shelf, with special reference to the eastern Bohai Sea. *Mar. Geol.* **145**, 225–253 (1998).
19. Saito, Y. et al. Transgressive and highstand systems tracts and post-glacial transgression, the East China Sea. *Sediment. Geol.* **122**, 217–232 (1998).
20. Uehara, K. & Saito, Y. Late Quaternary evolution of the Yellow/East China Sea tidal regime and its impacts on sediments dispersal and seafloor morphology. *Sediment. Geol.* **162**, 25–38 (2003).
21. Xu, T. et al. Understanding the formation mechanism of highly active ridges on East China Sea Shelf during the mid-late Holocene sea-level highstand. *Acta Oceanol. Sin.* **43**, 34–44 (2024).
22. Yang, C. S. Active, moribund and buried tidal sand ridges in the East China Sea and the Southern Yellow Sea. *Mar. Geol.* **88**, 97–116 (1989).
23. Anderson, J. B. et al. Recycling sediments between source and sink during a eustatic cycle: systems of late Quaternary northwestern Gulf of Mexico Basin. *Earth Sci. Rev.* **153**, 111–138 (2016).
24. Emery, K. O. Relict sediments on continental shelves of world. *Am. Assoc. Pet. Geol. Bull.* **52**, 445–464 (1968).
25. Hanebuth, T. J. J., Voris, H. K., Yokoyama, Y., Saito, Y. & Okuno, J. Formation and fate of sedimentary depocentres on Southeast Asia's Sunda Shelf over the past sea-level cycle and biogeographic implications. *Earth Sci. Rev.* **104**, 92–110 (2011).
26. Liu, J. P. et al. Fate of Ayeyarwady and Thanlwin Rivers sediments in the Andaman Sea and Bay of Bengal. *Mar. Geol.* **423**, 106137 (2020).
27. Milliman, J. D. & Farnsworth, K. L. *River Discharge to the Coastal Ocean: A Global Synthesis* (Cambridge University Press, 2011).
28. Li, G. et al. Sedimentary system response to the global sea level change in the East China Seas since the last glacial maximum. *Earth Sci. Rev.* **139**, 390–405 (2014).
29. Liu, J. et al. Late Pleistocene to Holocene facies architecture and sedimentary evolution of the Zhejiang coast, East China Sea. *Mar. Geol.* **459**, 107027 (2023).
30. Dou, Y. et al. Clay mineral evolution in the central Okinawa Trough since 28 ka: implications for sediment provenance and paleoenvironmental change. *Palaeogeogr. Palaeoclimatol. Palaeoecol.* **288**, 108–117 (2010).
31. Honda, M. C., Kusakabe, M., Nakabayashi, S. & Katagiri, M. Radiocarbon of sediment trap samples from the Okinawa trough: lateral transport of $^{14}$C-poor sediment from the continental slope. *Mar. Chem.* **68**, 231–247 (2000).
32. Oguri, K. et al. Evidence for the offshore transport of terrestrial organic matter due to the rise of sea level: the case of the East China Sea Continental Shelf. *Geophys. Res. Lett.* **27**, 3893–3896 (2000).
33. Meyer, V. D. et al. Dominant control of temperature on (sub-)tropical soil carbon turnover. *Nat. Commun.* **16**, 4530 (2025).
34. Wang, Y. et al. High rates of marine organic carbon burial on the southwest Greenland margin induced by Neoglacial advances. *Commun. Earth Environ.* **5**, 335 (2024).
35. Wu, J. et al. Deglacial release of petrogenic and permafrost carbon from the Canadian Arctic impacting the carbon cycle. *Nat. Commun.* **13**, 7172 (2022).
36. Zheng, L. et al. Climate-regulation of organic carbon export in erosive mountain settings: a case study from Taiwan since the last glacial maximum. *Quat. Sci. Rev.* **334**, 108687 (2024).
37. Dashtgard, S. E., Löwemark, L., Wang, P., Setiaji, R. A. & Vaucher, R. Geochemical evidence of tropical cyclone controls on shallow-marine sedimentation (Pliocene, Taiwan). *Geology* **49**, 566–570 (2021).
38. Chen, L. et al. Historical changes in organic matter input to the muddy sediments along the Zhejiang-Fujian Coast, China over the past 160 years. *Org. Geochem.* **111**, 13–25 (2017).
39. Xing, L., Zhang, H., Yuan, Z., Sun, Y. & Zhao, M. Terrestrial and marine biomarker estimates of organic matter sources and

distributions in surface sediments from the East China Sea shelf. *Cont. Shelf Res.* **31**, 1106–1115 (2011).
40. Lattaud, J. et al. The $C_{32}$ alkane-1,15-diol as a tracer for riverine input in coastal seas. *Geochim Cosmochim. Acta* **202**, 146–158 (2017).
41. Schouten, S., Hopmans, E. C. & Sinninghe Damsté, J. S. The organic geochemistry of glycerol dialkyl glycerol tetraether lipids: a review. *Org. Geochem.* **54**, 19–61 (2013).
42. Zhang, H. et al. East Asian hydroclimate modulated by the position of the westerlies during termination I. *Science* **362**, 580–583 (2018).
43. Liu, J. et al. Abrupt sea-level rise prior to the 8.2 ka climatic event revealed from the post-glacial sedimentary succession off the northern coast of Shandong Peninsula, North Yellow Sea. *Quat. Sci. Rev.* **363**, 109428 (2025).
44. Song, B. et al. Initiation of the Changjiang (Yangtze) delta and its response to the mid-Holocene sea level change. *Palaeogeogr. Palaeoclimatol. Palaeoecol.* **388**, 81–97 (2013).
45. Liu, X. et al. Sedimentary pyrites and C/S ratios of mud sediments on the East China Sea inner shelf indicate late Pleistocene-Holocene environmental evolution. *Mar. Geol.* **450**, 106854 (2022).
46. Yang, S. et al. Burial of organic carbon in Holocene sediments of the Zhujiang (Pearl River) and Changjiang (Yangtze River) estuaries. *Mar. Chem.* **123**, 1–10 (2011).
47. Jiang, J. et al. Meltwater contribution to lake water budget in mid-latitude Asia during the deglaciation and early Holocene. *Geophys. Res. Lett.* **49**, e2022GL100229 (2022).
48. Liu, J. et al. Pre-aged terrigenous organic carbon biases ocean ventilation-age reconstructions in the North Atlantic. *Nat. Commun.* **14**, 3788 (2023).
49. Eglinton, T. I. et al. Climate control on terrestrial biospheric carbon turnover. *Proc. Natl. Acad. Sci. USA*. **118**, e2011585118 (2021).
50. Wang, H. et al. Damming alters the particulate organic carbon sources, burial, export and estuarine biogeochemistry of rivers. *J. Hydrol.* **607**, 127525 (2022).
51. Lan, K. et al. Changes in chemical weathering regime of shelf sediments of the East China sea controlled by sea-level and climatic changes since the last deglaciation. *J. Asian Earth Sci.* **268**, 106169 (2024).
52. Yang, C. et al. Lithium isotopic constraints on systematic biases in reconstructing continental weathering processes from bulk sedimentary records at continental margins. *Glob. Planet. Change* **253**, 104942 (2025).
53. Liu, H. et al. A 13,000-year peatland palaeohydrological response to the ENSO-related Asian monsoon precipitation changes in the middle Yangtze Valley. *Quat. Sci. Rev.* **212**, 80–91 (2019).
54. Li, C. et al. The time scale of river sediment source-to-sink processes in East Asia. *Chem. Geol.* **446**, 138–146 (2016).
55. Inthorn, M., Wagner, T., Scheeder, G. & Zabel, M. Lateral transport controls distribution, quality, and burial of organic matter along continental slopes in high-productivity areas. *Geology* **34**, 205–208 (2006).
56. Kang, S. et al. Early Holocene weakening and mid- to late Holocene strengthening of the East Asian winter monsoon. *Geology* **48**, 1043–1047 (2020).
57. Qiu, J. et al. Mechanism and genesis of Sanmen Bay as a sink of Holocene Yangtze River sediment, Zhejiang Province, China. *Front. Earth Sci.* **11**, 1329921 (2024).
58. Li, Y. et al. Tracing the Changjiang-derived sediments along the southeast coast of China during the Holocene. *Glob. Planet. Change* **248**, 104770 (2025).
59. Kim, S. et al. Bioturbation supplying young carbon into West Antarctic continental margin sediment. *Palaeogeogr. Palaeoclimatol. Palaeoecol.* **602**, 111161 (2022).
60. Sun, X. et al. Sediment resuspension accelerates the recycling of terrestrial organic carbon at a large river coastal ocean interface. *Glob. Biogeochem. Cycles* **38**, e2024GB008213 (2024).
61. Magill, C. R. et al. Transient hydrodynamic effects influence organic carbon signatures in marine sediments. *Nat. Commun.* **9**, 4690 (2018).
62. Schefuß, E. et al. Hydrologic control of carbon cycling and aged carbon discharge in the Congo River basin. *Nat. Geosci.* **9**, 687–690 (2016).
63. Soulet, G., Skinner, L. C., Beaupré, S. R. & Galy, V. A note on reporting of reservoir $^{14}C$ disequilibria and age offsets. *Radiocarbon* **58**, 205–211 (2016).
64. Liu, X. et al. Sediment resuspension as a driving force for organic carbon transference and rebalance in marginal seas. *Water Res.* **257**, 121672 (2024).
65. Bianchi, T. S. & Canuel, E. A. *Chemical Biomarkers in Aquatic Ecosystems* (Princeton University Press, 2012).
66. Tesi, T. et al. Massive remobilization of permafrost carbon during post-glacial warming. *Nat. Commun.* **7**, 13653 (2016).
67. Dong, J. et al. Holocene climate modulates mud supply, transport, and sedimentation on the East China Sea shelf. *J. Geophys. Res. Earth Surf.* **125**, e2020JF005731 (2020).
68. Shen, X. et al. Reconstruction of Kuroshio intrusion into the South China Sea over the last 40 kyr. *Quat. Sci. Rev.* **290**, 107622 (2022).
69. Li, G. et al. Dam-triggered organic carbon sequestration makes the Changjiang (Yangtze) river basin (China) a significant carbon sink. *J. Geophys. Res. Biogeosci.* **120**, 39–53 (2015).
70. Bao, R. et al. Widespread dispersal and aging of organic carbon in shallow marginal seas. *Geology* **44**, 791–794 (2016).
71. Cong, J. et al. The climate-driven mechanisms of sedimentary evolution in the mud area southwest off Cheju Island during the Holocene. *Palaeogeogr. Palaeoclimatol. Palaeoecol.* **676**, 113127 (2025).
72. Liu, J. et al. Formation of the Yangtze Shoal in response to the post-glacial transgression of the paleo-Yangtze (Changjiang) estuary, China. *Mar. Geol.* **423**, 106080 (2020).
73. Pang, C., Li, K. & Hu, D. Net accumulation of suspended sediment and its seasonal variability dominated by shelf circulation in the Yellow and East China Seas. *Mar. Geol.* **371**, 33–43 (2016).
74. de Haas, H., van Weering, T. C. E. & de Stigter, H. Organic carbon in shelf seas: sinks or sources, processes and products. *Cont. Shelf Res.* **22**, 691–717 (2002).
75. Chen, J. et al. Physical mechanisms of sediment trapping and deposition on spatially confined mud depocenters in high-energy shelf seas. *J. Geophys. Res. Oceans* **130**, e2025JC022622 (2025).
76. Moy, C. M., Seltzer, G. O., Rodbell, D. T. & Anderson, D. M. Variability of El Niño/Southern Oscillation activity at millennial timescales during the Holocene epoch. *Nature* **420**, 162–165 (2002).
77. Dykoski, C. A. et al. A high-resolution, absolute-dated Holocene and deglacial Asian monsoon record from Dongge Cave, China. *Earth Planet. Sci. Lett.* **233**, 71–86 (2005).
78. Feng, Z. et al. Spatial and temporal variations and controlling factors of sediment accumulation in the Yangtze River estuary and its adjacent sea area in the Holocene, especially in the Early Holocene. *Cont. Shelf Res.* **125**, 1–17 (2016).
79. Kang, S., Wang, X., Du, J. & Song, Y. Paleoclimates inform on a weakening and amplitude-reduced East Asian winter monsoon in the warming future. *Geology* **50**, 1224–1228 (2022).
80. Yang, H. et al. The intensifying East China Sea Kuroshio and disappearing Ryukyu Current in a warming climate. *Geophys. Res. Lett.* **51**, e2023GL106944 (2024).
81. Martens, J. et al. Remobilization of dormant carbon from Siberian-Arctic permafrost during three past warming events. *Sci. Adv.* **6**, eabb6546 (2020).
82. Mollenhauer, G., Schneider, R. R., Müller, P. J., Spieß, V. & Wefer, G. Glacial/interglacial variablity in the Benguela upwelling system: spatial distribution and budgets of organic carbon accumulation. *Glob. Biogeochem. Cycles* **16**, 1134 (2002).

83. Galy, V. et al. Efficient organic carbon burial in the Bengal fan sustained by the Himalayan erosional system. *Nature* **450**, 407–410 (2007).
84. Berné, S., Jouet, G., Bassetti, M. A., Dennielou, B. & Taviani, M. Late Glacial to Preboreal sea-level rise recorded by the Rhône deltaic system (NW Mediterranean). *Mar. Geol.* **245**, 65–88 (2007).
85. Köhler, P., Nehrbass-Ahles, C., Schmitt, J., Stocker, T. F. & Fischer, H. A 156 kyr smoothed history of the atmospheric greenhouse gases $CO_2$, $CH_4$, and $N_2O$ and their radiative forcing. *Earth Syst. Sci. Data* **9**, 363–387 (2017).
86. Reimer, P. J. et al. The IntCal20 northern hemisphere radiocarbon age calibration curve (0–55 cal kBP). *Radiocarbon* **62**, 725–757 (2020).
87. Versteegh, G. J. M., Bosch, H.-J. & De Leeuw, J. W. Potential palaeoenvironmental information of $C_{24}$ to $C_{36}$ mid-chain diols, keto-ols and mid-chain hydroxy fatty acids; a critical review. *Org. Geochem.* **27**, 1–13 (1997).
88. Wang, Y. et al. Improved protocols for large-volume injection and liquid chromatography–mass spectrometry analyses enable determination of various glycerol dialkyl glycerol tetraethers in a small amount of sediment and suspended particulate matter. *Chem. Geol.* **595**, 120793 (2022).
89. Chen, L. et al. New insights into the Holocene temperature conundrum from long-chain alkyl diol paleothermometers in the East China Sea inner shelf. *Palaeogeogr. Palaeoclimatol. Palaeoecol.* **675**, 113093 (2025).
90. Clark, R. C. & Blumer, M. Distribution of *n*-paraffins in marine organisms and sediment. *Limnol. Oceanogr.* **12**, 79–87 (1967).
91. Zhang, H. T., Zhang, X. H. & Wen, Z. H. *Geological and Geophysical Map Series of Eastern China Seas and Adjacent Regions: Sediments Distribution Map* (China Ocean Press, 2012).
92. Guan, B. & Fang, G. Winter counter-wind currents off the southeastern China coast: A review. *J. Oceanogr.* **62**, 1–24 (2006).
93. Lamb, A. L., Wilson, G. P. & Leng, M. J. A review of coastal palaeoclimate and relative sea-level reconstructions using $\delta^{13}C$ and C/N ratios in organic material. *Earth Sci. Rev.* **75**, 29–57 (2006).
94. Gao, C. et al. Anthropogenic impact on the organic carbon sources, transport and distribution in a subtropical semi-enclosed bay. *Sci. Total Environ.* **767**, 145047 (2021).
95. Wu, Y., Eglinton, T. I., Zhang, J. & Montlucon, D. B. Spatiotemporal variation of the quality, origin, and age of particulate organic matter transported by the Yangtze River (Changjiang). *J. Geophys. Res. Biogeosci.* **123**, 2908–2921 (2018).
96. Lambeck, K., Rouby, H., Purcell, A., Sun, Y. & Sambridge, M. Sea level and global ice volumes from the last glacial maximum to the Holocene. *Proc. Natl. Acad. Sci. USA*. **111**, 15296–15303 (2014).
97. Abdul, N. A., Mortlock, R. A., Wright, J. D. & Fairbanks, R. G. Younger Dryas sea level and meltwater pulse 1B recorded in Barbados reef crest coral *Acropora palmata*. *Paleoceanography* **31**, 330–344 (2016).
98. Rasmussen, S. O. et al. A new Greenland ice core chronology for the last glacial termination. *J. Geophys. Res.* **111**, D06102 (2006).
99. Ellison, C. R. W., Chapman, M. R. & Hall, I. R. Surface and deep ocean interactions during the cold climate event 8200 years ago. *Science* **312**, 1929–1932 (2006).
100. Ning, X., Liu, Z., Cai, Y., Fang, M. & Chai, F. Physicobiological oceanographic remote sensing of the East China Sea: satellite and in situ observation. *J. Geophys. Res. Oceans* **103**, 21623–21635 (1998).



## Acknowledgements
We thank Huang Huang, Jingrui Li, Hao Wei, and Zhimeng Zhuang for insightful discussions. We also appreciate the editors and anonymous reviewers for their help and constructive comments on the manuscript.


## Author contributions
L.C. and J.L. designed the study. J.Q. and X.H. helped collect the core materials. L.C., F.L., S.S., and X.H. carried out the laboratory work. L.C. and J.L. analyzed proxy data. L.C. wrote the manuscript with contributions from all authors. Y.S., B.C., G.T., and M.Q. contributed to data interpretation and manuscript refinement.


## Funding
This work has been financed by the National Natural Science Foundation of China (Grant Nos. 42576080 and 41906062 to J.L. and L.C.), the China-ASEAN (Association of Southeast Asian Nations) maritime cooperation fund (Asian Cooperation Fund: Cooperative Research on Marine Geological Environment and Disasters in the Yangtze River Delta and Red River Delta to J.L.), the China Postdoctoral Science Foundation Funded Project (Grant No. 2018M642622 to L.C.), and the Shandong Provincial Postdoctoral Innovation Project Special Funding Project (Grant No. 201903051 to L.C.).


## Competing interests
The authors declare no competing interests.

## Additional information
**Supplementary information** The online version contains supplementary material available at https://doi.org/10.1038/s43247-026-03645-2.


**Correspondence** and requests for materials should be addressed to Jian Liu.



**Peer review information** *Communications Earth and Environment* thanks the anonymous reviewers for their contribution to the peer review of this work. Primary handling editors: Somaparna Ghosh. A peer review file is available.